remote sensing

MDPI

Article

Measuring Vegetation Height in Linear Disturbances in the Boreal Forest with UAV Photogrammetry

Shijuan Chen [1,2,*], Gregory J. McDermid [1], Guillermo Castilla [3] and Julia Linke [1]

[1] Department of Geography, University of Calgary, Calgary, AB T2N 1N4, Canada; mcdermid@ucalgary.ca (G.M.); julia.linke@ucalgary.ca (J.L.)
[2] Department of Earth and Environment, Boston University, 685 Commonwealth Avenue, Boston, MA 02215, USA
[3] Northern Forestry Centre, 5320 122 Street Northwest, Edmonton, AB T6H 3S5, Canada; guillermo.castilla@canada.ca
* Correspondence: shijuan.chen@ucalgary.ca; Tel.: +1-(617)-358-0503

Received: 16 October 2017; Accepted: 29 November 2017; Published: 3 December 2017

Abstract: Monitoring vegetation recovery typically requires ground measurements of vegetation height, which is labor-intensive and time-consuming. Recently, unmanned aerial vehicles (UAVs) have shown great promise for characterizing vegetation in a cost-efficient way, but the literature on specific methods and cost savings is scant. In this study, we surveyed vegetation height on seismic lines in Alberta's Boreal Forest using a point-intercept sampling strategy, and compared them to height estimates derived from UAV-based photogrammetric point clouds. In order to derive UAV-based vegetation height, we tested three different approaches to estimate terrain elevation: (1) UAV_RTK, where photogrammetric point clouds were normalized using terrain measurements obtained from a real-time kinematic global navigation satellite system (RTK GNSS) surveys; (2) UAV_LiDAR, where photogrammetric data were normalized using pre-existing LiDAR (Light Detection and Ranging) data; and (3) UAV_UAV, where UAV photogrammetry data were used alone. Comparisons were done at two scales: point level (n = 1743) and site level (n = 30). The point-level root-mean-square errors (RMSEs) of UAV_RTK, UAV_LiDAR, and UAV_UAV were 28 cm, 31 cm, and 30 cm, respectively. The site-level RMSEs were 11 cm, 15 cm, and 8 cm, respectively. At the aggregated site level, we found that UAV photogrammetry could replace traditional field-based vegetation surveys of mean vegetation height across the range of conditions assessed in this study, with an RMSE less than 10 cm. Cost analysis indicates that using UAV-based point clouds is more cost-effective than traditional field vegetation surveys.

Keywords: UAV; vegetation; point clouds; 3D; accuracy assessment; remote sensing

1. Introduction

The rapid development of natural resource extraction in Alberta, Canada, has created large numbers of anthropogenic disturbance features, such as roads, seismic lines, pipelines, and well sites, which have cumulative effects on wildlife habitat and biodiversity. In Alberta's Boreal Forest, populations of woodland caribou (*Rangifer tarandus caribou*) are threatened because of habitat disturbance due in part to industrial development [1], as well as other factors [2]. Studies have shown that linear disturbances are both directly and indirectly linked to the decline of these populations [3,4]. For example, linear features increase the spatial overlap between caribou and wolves, their main predator, and provide movement corridors for wolf packs to travel and hunt more efficiently [5]. Indirectly, linear features also provide forage and access for adaptable ungulates, such as moose, elk, and deer. These species would otherwise not be prominent in caribou habitat, and their presence in turn increases the carrying capacity for wolves and other predators [6,7]. Among the linear disturbances

present in the Boreal Forest, seismic lines—narrow corridors created to deploy seismic equipment for geophysical exploration—have the greatest impact on caribou in Alberta, because of their very slow reforestation rates, high density (up to 10 km per km^2), and wide distribution [8].

To mitigate these negative ecological effects, both regulators and industry are making efforts to assess and enhance vegetation recovery on seismic lines through active reclamation and monitoring activities. Measuring vegetation recovery status on seismic lines is important, because certain vegetation metrics, such as height and species composition, are related to behavioral or population responses in the predator–prey system [9]. These metrics can inform the determination of whether a seismic line has recovered or not. For example, a Golder Associates study showed that caribou preferentially select seismic lines with vegetation higher than 1.5 m [10], and Van Rensen et al. [8] suggested using a 3-m vegetation height to define a recovered seismic line, based on the minimum regeneration height required by Alberta's forestry ground rules [11].

Traditionally, vegetation height is measured in the field by trained technicians using handheld instruments, such as hypsometers (for mature trees) or measuring poles (for seedlings and low vegetation). However, this time-consuming activity is expensive and difficult to scale [12]. Remote sensing provides an attractive means of collecting data that reduces the amount of fieldwork, with a demonstrated capacity to measure vegetation attributes quickly and effectively at a variety of scales [13–16]. In particular, three-dimensional (3D) remote-sensing technologies, such as light detection and ranging (LiDAR), can accurately estimate horizontal and vertical vegetation structure [17,18]. As an active form of remote-sensing technology, LiDAR has the ability to penetrate canopies and can therefore capture the complete vertical profile of vegetation [19–21]. However, LiDAR acquisitions are expensive; in particular, data sets with densities high enough to characterize fine-scale structural attributes of vegetation on narrow linear-disturbance features, such as 5–8 m wide seismic lines, have high associated costs. This factor is exacerbated in vegetation recovery monitoring programs, which require repeated observations over time. As a result, there is strong interest in developing low-cost remote sensing techniques such as those based on unmanned aerial vehicles (UAVs, also known as drones).

UAVs carrying imaging systems are capable of acquiring data with high spatial and temporal resolutions [22–24]. A sequence of overlapping images collected by a UAV can be used to generate high-density point clouds through modern structure-from-motion (SfM) workflows [25], thus providing information on both the horizontal and vertical profiles of vegetation [26,27]. Compared to LiDAR acquired from piloted aircraft, point clouds derived from UAV photogrammetry have lower cost, more flexible flight planning, and much greater point densities [28–30]. Although some studies have documented relatively lower accuracy of vegetation structural variables estimated with this technique [26,31], UAV photogrammetry provides a promising avenue for vegetation-recovery monitoring on small anthropogenic disturbance features, and could potentially replace traditional field surveys under certain conditions.

The goal of this study was to develop and evaluate a method of estimating vegetation height on linear disturbances in the Boreal Forest using point clouds derived from UAV photogrammetry, and to assess the accuracy and cost of various application scenarios. In particular, we wanted to know whether point clouds from UAV photogrammetry provide an effective means of complementing—or even replacing—traditional ground surveys of vegetation height. The primary limitation of UAV photogrammetry, a passive technology with limited ability to penetrate the canopy, involves difficulty in reliably capturing terrain elevation in vegetated areas, unlike active remote-sensing technologies such as LiDAR. To examine this factor, we assessed three different methods of normalizing point clouds (i.e., subtracting the terrain elevation from the z of each photogrammetric point):

(1) UAV_RTK, where point clouds are normalized using terrain elevation measured with a survey-grade real-time kinematic (RTK) global navigation satellite system (GNSS) receiver in the field;

(2) UAV_LiDAR, where photogrammetric point clouds are normalized using spatially coincident pre-existing LiDAR data; and
(3) UAV_UAV, where terrain elevation is estimated from the UAV photogrammetry data alone.

We compared vegetation height estimates derived from each of these methods to a reference dataset consisting of ground-measured vegetation height across nearly 2000 point-intercept samples collected on 30 experimental sites, representing seismic lines at various stages of recovery. Comparisons were done at two scales: point level and site level.

2. Materials and Methods

2.1. Study Area

This research was conducted across four study areas in northeastern Alberta, Canada (Figure 1), which represent a range of boreal environments (Figure 2). We visited a total of 30 experimental sites, each located on an individual seismic line. The surveyed seismic lines are under the process of natural regeneration, and have not been actively restored. The first study area, about 1000 km^2 in size, is located near the town of Anzac (central coordinates: 56°21′23.43″, −111°16′54.1″) and included a range of poor-mesic, medium-mesic, and medium-hygric sites. The second study area, about 400 km^2 in size, is located south of Conklin (central coordinates: 55°26′56.07″, −110°47′58.28″), and included mainly poor-hydric, medium-hydric, medium-hygric, poor-mesic, and medium-mesic sites. The third study area, about 450 km^2 in size, is located near the town of Lac La Biche (central coordinates: 54°59′55.35″, −111°52′49.70″), and is composed of medium-mesic and poor-xeric sites. The fourth study area, about 380 km^2 in size, is located north of Fort MacKay (central coordinates: 57°31′56.42″, −111°16′14.75″), and contained mainly poor-xeric sites. All four study areas are located in the Boreal Forest natural region, which is characterized by a mixture of upland and wetland vegetation communities on gently undulating terrain [32]. Upland areas were generally forested with deciduous, coniferous, and mixedwood stands, whereas lowland areas were comprised of fens and bogs. The main vegetation species were trembling aspen (*Populus tremuloides*), black spruce (*Picea mariana*), paper birch (*Betula papyrifera*), and jack pine (*Pinus banksiana*) as trees, and green alder (*Alnus crispa*) and willow (*Salix* spp.) as shrubs. Although the seismic lines in the four areas may have had different vegetation-recovery status, most were found to have relatively low vegetation height (less than 1.0 m on average).

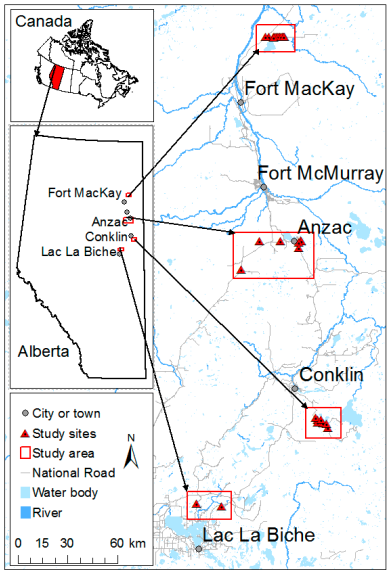

Figure 1. Location of the 30 surveyed sites, distributed among four study areas in the Boreal Forest natural region of northeastern Alberta, Canada.

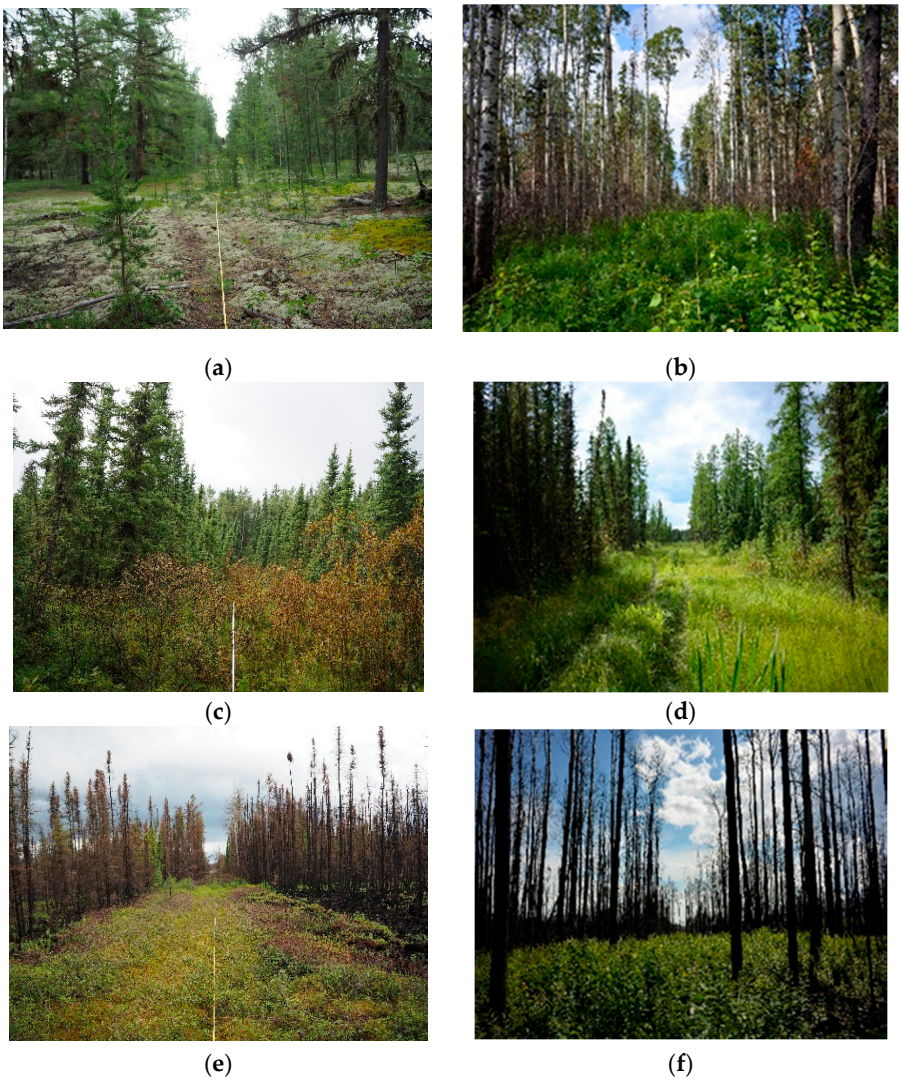

Figure 2. Some of the boreal environments surveyed: (**a**) poor-xeric site, dominated by jack pine (*Pinus banksiana*) with an understory of lichen; (**b**) medium-mesic site, dominated by trembling aspen (*Populus tremuloides*); (**c**) medium-hydric site, dominated by black spruce (*Picea mariana*) and willow (*Salix* spp.); (**d**) poor-hydric site, dominated by black spruce and graminoids; (**e**) poor-mesic site, dominated by black spruce with understory of Labrador tea (*Rhododendron groenlandicum*) and feather moss (*Hylocomium splendens*); and (**f**) post-fire forest, dominated by trembling aspen.

2.2. Field Measurements

We used a point-intercept sampling strategy to select the location of individual measurement stations within an experimental site (i.e., a seismic line; Figure 3). At each site, a long transect spanning 150 m was set up using measuring tapes. From the start of the long transect to the 60-m point, we placed measurement stations every 10 m. From the 60-m point to the 90-m point, we took measurements every 1 m. From the 90-m point to the end point (at 150 m), we took measurements every 10 m. For each seismic line in the first three study areas (total of 16 sites), three additional cross-line transects spanning 6 m were set up perpendicular to the long transect, at the 60-m, 75-m, and 90-m points, respectively. On these cross-line transects, we made measurements every 0.5 m.

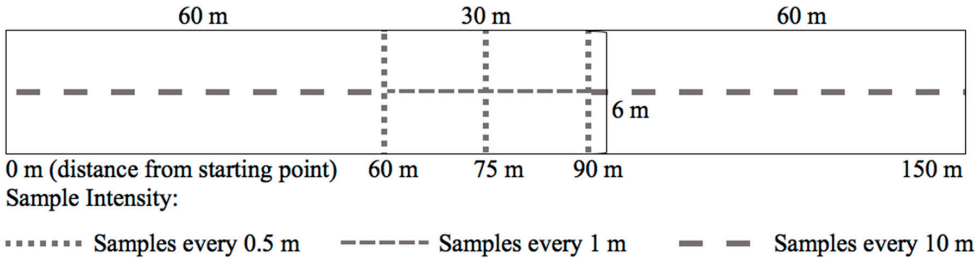

Figure 3. Vegetation height sampling using a point-intercept strategy on a 150 m × 6 m plot on a seismic line.

At each station, we measured top vegetation height and the 3D coordinates of the ground point: easting and northing in Universal Transverse Mercator (UTM) zone 12, North American Datum of 1983 (NAD83), plus terrain elevation. Vegetation height was determined with a measuring pole. The pole, which was marked every 5 cm, was placed vertically on the ground at each measurement station. If any vegetation parts touched the pole, the height of the point where it touched was recorded to the closest pole mark (Figure 4). In cases where multiple touches of vegetation occurred, only the maximum height was recorded. When vegetation height was equal to or larger than 3 m, we were not able to hold the measuring pole exactly vertically to touch the vegetation and read the height measurements of the pole accurately. Thus, to ensure accurate and reliable field measurements of vegetation heights, we discarded data from a handful of stations where vegetation height was equal to or greater than 3.0 m. This height (3.0 m) coincides with the minimum regeneration height required by Alberta's forestry ground rules [11]. Following this procedure, a total of 1743 stations were measured by field personnel in the summer (leaf-on season) of 2016. Summary statistics of the field vegetation heights recorded are presented in Table 1.

The coordinates of each measurement station were determined with real-time kinematic global navigation satellite system (RTK GNSS) survey techniques, which can achieve decimeter-level accuracies [33]. RTK surveys measure the position of a rover relative to its base station in real time, where the base station is placed at a fixed location with a clear view of the sky. We used precise point positioning (PPP) post-processing to improve the accuracy of the original RTK measurements, as follows. First, raw observations of the base station were recorded during the survey. Then, the Canadian Spatial Reference System PPP online application was used to refine the absolute positions of the base station. Differences between the original and PPP coordinates of the base station were then computed. Finally, we applied a 3D shift based on the computed differences for each site. PPP post-processing can achieve absolute positioning accuracies of 10 cm or better.

2.3. UAV Imagery Acquisition

A lightweight UAV quadcopter platform, the 3D Robotics Iris, was used to perform image acquisition. Mission Planner, a free, open-source software package, was used for flight planning. Flight specifications were as follows: altitude, 42 m; speed, 3 m/s; forward overlap, 90%; and side overlap, 71%. The flight pattern, shown in Figure 5, was designed to maximize photographic overlap along the measurement stations. Each flight consisted of 12 passes which were 64 m long and 15 m apart, oriented perpendicular to the seismic line. Each flight covered at least 180 m × 64 m on the ground, and took about 15 min to complete.

Table 1. Vegetation height statistics for the 1743 sample points measured in this study (obtained by point-intercept sampling on 30 seismic lines).

Study Area [1]	Site ID	Sample Size	Mean Height (m)	Maximum Height (m)	Minimum Height (m)	Range (m)	Standard Deviation (m)
FMK	201	43	0.15	0.6	0	0.6	0.18
FMK	202	43	0.03	0.5	0	0.5	0.09
FMK	203	43	0.10	0.5	0	0.5	0.14
FMK	204	42	0.18	1.2	0	1.2	0.29
FMK	205	43	0.02	0.25	0	0.25	0.05
FMK	218	37	0.00	0.05	0	0.05	0.01
FMK	219	43	0.01	0.1	0	0.1	0.02
FMK	227	43	0.01	0.1	0	0.1	0.02
FMK	235	43	0.24	1.85	0	1.85	0.38
FMK	239	43	0.16	0.7	0	0.7	0.18
FMK	246	43	0.14	0.7	0	0.7	0.22
FMK	247	43	0.20	2.3	0	2.3	0.39
FMK	248	43	0.26	1.2	0	1.2	0.23
FMK	298	43	0.02	0.5	0	0.5	0.09
LLB	301	47	1.44	2.9	0	2.9	0.99
LLB	305	65	0.22	2.95	0	2.95	0.63
ANZ	306	78	0.25	0.6	0	0.6	0.15
ANZ	307	78	0.47	1.4	0.05	1.35	0.25
ANZ	308	79	0.32	1.4	0	1.4	0.27
ANZ	309	73	0.67	2	0	2	0.53
ANZ	310	45	0.38	1.9	0	1.9	0.39
ANZ	311	75	0.18	1.5	0	1.5	0.29
ANZ	312	73	0.19	1.2	0	1.2	0.18
CNK	314	78	0.15	0.8	0	0.8	0.13
CNK	315	77	0.33	2.9	0.05	2.85	0.32
CNK	316	66	0.56	2.4	0.05	2.35	0.46
CNK	317	79	0.26	0.75	0	0.75	0.16
CNK	318	78	0.34	0.95	0	0.95	0.19
CNK	320	79	0.40	2.35	0	2.35	0.33
CNK	321	78	0.51	1.2	0.1	1.1	0.20
All	NA	1743	0.30	2.95	0	2.95	0.42

[1] FMK refers to the study area near Fort MacKay; LLB refers to the study area near Lac La Biche; ANZ refers to the study area near Anzac; and CNK refers to the study area near Conklin.

A consumer-grade Nikon COOLPIX A digital camera (RGB [Red, Green and Blue]) with an 18.5-mm focal length NIKKOR lens was mounted under the UAV. Camera configurations were set as follows: mode, TAv; intervalometer, 1 frame/s; aperture, F2.8; shutter speed, 1/2500; ISO, auto with NR disabled; white balance, manual, calibrated against field reference at each site; resolution, L/3:2 (4928 $\times$ 3264 effective); and focus, infinity (i.e., 4 m to infinity).

Each site had nine ground control points (GCPs) established for positional reference. Three of the GCPs were laid out along the seismic line, and an additional six were laid out in the adjacent forest at locations visible from the air. GCPs were marked on the ground using high-visibility flagging tape, and the coordinates were measured by RTK GNSS with PPP post-processing.

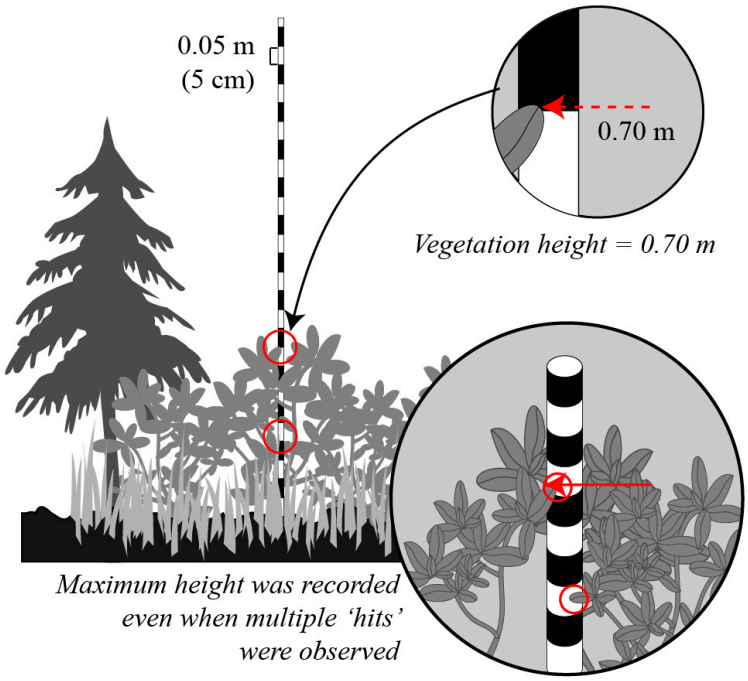

Figure 4. Vegetation height measurement at a sample point (modified from [34]).

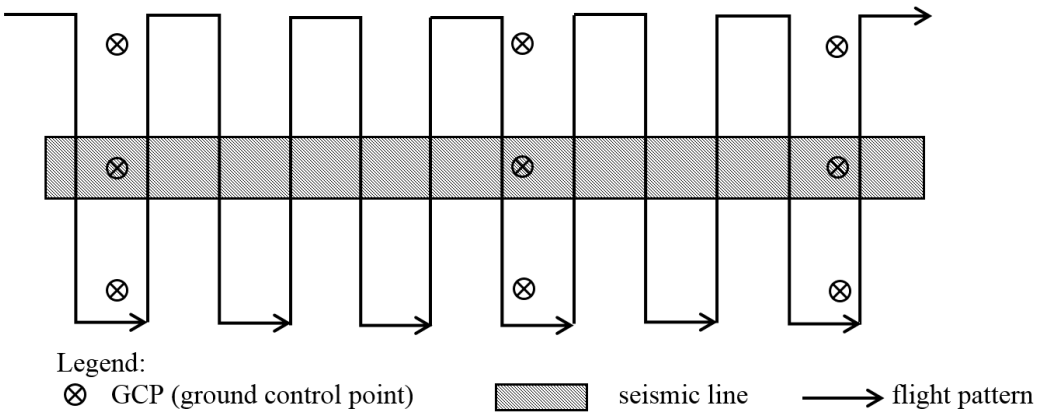

Figure 5. Unmanned aerial vehicle (UAV) flight pattern and GCP distribution.

2.4. Generation and Geo-Reference of Point Clouds

We used a commercial software package, Agisoft PhotoScan Professional Edition, version 1.2.4 [35], to generate dense point clouds through an automated set of procedures based on the structure-from-motion (SfM) workflow. SfM reconstructs the 3D structure of a scene from a sequence of overlapping images. With this technique, the geometry of the scene, camera positions, and orientation can be solved automatically without a-priori knowledge of the camera's 3D position and orientation [36–38]. An overview of the workflow used to generate dense point clouds is shown as Figure 6. First, we removed images captured during takeoff and landing, and loaded the remaining images into the software. Second, we aligned the images using the following parameters: accuracy, high; pair pre-selection, disabled; key point limit, 4000; and tie point limit, 4000. Third, we resolved the relative camera positions and generated sparse point clouds. Fourth, we generated dense point clouds using the following configuration: quality, medium; and depth filtering method, aggressive. Fifth, we used a guided approach for marker (i.e., GCP) projection in PhotoScan. Markers were automatically placed on individual photos and then refined manually. Sixth, we entered the geographic

coordinates and elevation of the GCPs and re-generated the dense point clouds. Finally, we exported the geo-referenced point clouds to LAS format for further processing. A perspective view of a sample point cloud from one of the experimental sites is shown in Figure 7.

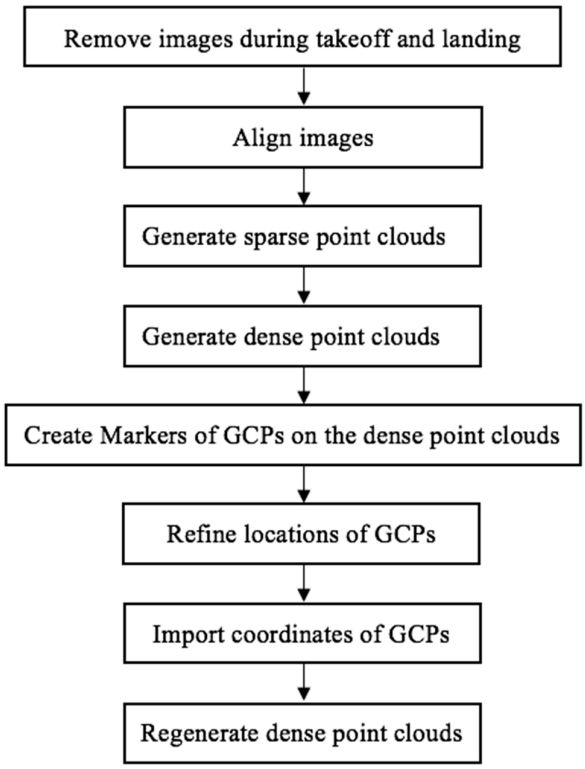

Figure 6. Workflow of generating and geo-referencing point clouds.

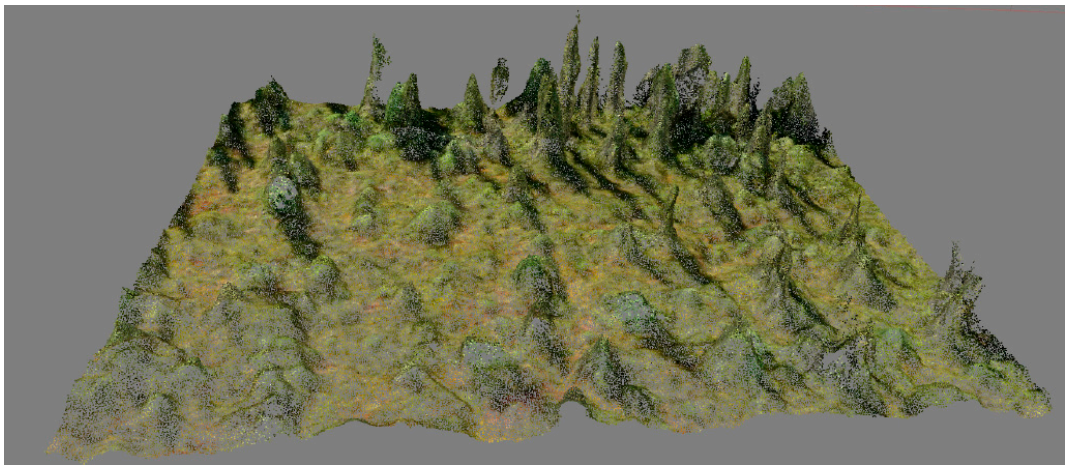

Figure 7. Rendering of a dense sample point cloud from one of the experimental sites.

2.5. LiDAR Data

LiDAR data for the Anzac study area were provided by the Alberta's Oil Sands Projects. This data set was acquired by fixed-wing aircraft in August 2013. The average point density of this data set was close to 10 points per m^2. LiDAR data for the other study areas were provided by the Government of Alberta. These data sets were acquired between 2010 and 2012, and also contained point densities of

about 10 points per m^2. The relative and absolute vertical accuracies of these data sets were 15 cm and 30 cm, respectively.

2.6. Vegetation-Height Estimates

To save computational time during later processing, the geo-referenced UAV-based point clouds were clipped with a 3-m circular buffer around each sample point (station) using LAStools (rapidlasso GmbH, Gilching, Germany) [39]. Then, we used three different methods to estimate vegetation height: UAV_RTK, UAV_LiDAR, and UAV_UAV (Figure 8). For each of the methods, vegetation height at a sample point was estimated as the top value minus an estimate of terrain elevation. For the three methods, the top values were the same, but the strategies for estimating terrain elevations were different. For a sample point with RTK-measured ground coordinates (x_r, y_r, z_r), the top value was defined as the 99th percentile of z values of the UAV-based points (x_i, y_i, z_i) whose horizontal distance d_i to the sample point was less than a top-search radius (TSR). After testing different values (see Section 3.4 for details), we chose 0.2 m as the TSR. Given the positioning accuracy of the RTK measurements, the true location of any given sample point was expected to be within this circle 19 times out of 20.

$$d_i = \sqrt{(x_r - x_i)^2 + (y_r - y_i)^2} \quad (1)$$

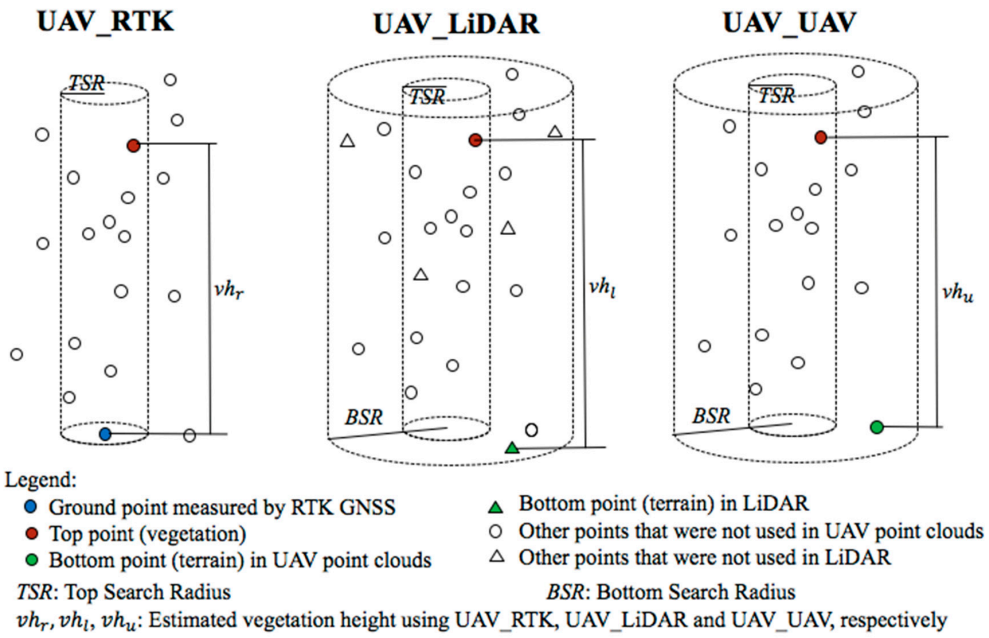

Figure 8. Three methods of estimating vegetation height: UAV_RTK (photogrammetric heights normalized with real-time-kinematic global navigation satellite system data measured in the field), UAV_LiDAR (photogrammetric heights normalized with pre-existing light detection and ranging data), and UAV_UAV (no external data used for normalization). RTK GNSS: real-time kinematic global navigation satellite system.

For the UAV_RTK method, terrain elevation (z_r) at the sample point was simply z_r, as measured in the field. For the UAV_LiDAR method, terrain elevation was estimated as the minimum of z values of the supplementary LiDAR points (x_i, y_i, z_i) within a bottom-search radius (BSR). We also tested an alternative method whereby z_r was set to the z of the closest LiDAR point among those classified as bare ground, but this produced slightly worse results. For the UAV_UAV method, terrain elevation was estimated as the minimum of z values of the UAV-based points (x_i, y_i, z_i) within a BSR. Terrain within the surveyed sites was relatively flat and smooth, which allowed for a relatively wide BSR to

be used. To ascertain which radius would be most suitable for our study, we computed the site-level root-mean-square error (RMSE) of vegetation height estimates derived from different values of BSR, ranging from 25 cm to 3 m, with steps of 25 cm. Once the best BSR had been chosen, we also wanted to investigate whether our choice of 20 cm for the TSR could have been improved with a similar strategy or not. To establish this, we tested a series of TSR distances, starting at 5 cm and proceeding to 30 cm at 5-cm intervals. These distances (5 cm and 30 cm) are equivalent to 0.5 and 3 times the horizontal positional accuracy of the RTK measurements, respectively.

2.7. Comparison and Accuracy Assessment

To assess the three different methods employed to estimate vegetation height from the UAV point clouds, we computed *RMSE*, *Normalized RMSE*, and *Bias* of the height estimates using the following equations:

$$RMSE = \sqrt{\frac{\sum_{i=1}^{n}\left(h_i - \hat{h_i}\right)^2}{n}} \quad (2)$$

$$Normalized\ RMSE = \frac{RMSE}{h_{max} - h_{min}} \quad (3)$$

$$Bias = \frac{\sum_{i=1}^{n}\left(h_i - \hat{h_i}\right)}{n} \quad (4)$$

where h_i and $\hat{h_i}$ were the ground-measured and UAV-estimated vegetation heights at sample point i, respectively, and $h_{max} - h_{min}$ was the site-specific range of vegetation height. We computed accuracy statistics at both the point level (n = 1743) and aggregated site level (n = 30) for vegetation height estimates. At point level, we also computed accuracy statistics by height strata: Stratum I (low), 0–0.5 m; stratum II (medium), 0.51–2.0 m; and stratum III (high), >2.0 m. These height strata are commonly used in field protocols of ecological recovery monitoring of disturbed features in Alberta [36]. In addition, we created multiple vertical-profile graphs (one profile per method, plus the ground measurements) of some of the transects for visual comparisons.

2.8. Cost Analysis

We estimated the cost that a company would incur for surveying an area similar to that in this study, under three scenarios: (1) traditional vegetation survey with standard measurement tools (hypsometers and measurement poles), (2) UAV photogrammetry surveys with supplementary LiDAR (analogous to our UAV_LiDAR method), and (3) stand-alone UAV photogrammetry surveys (analogous to our UAV_UAV method). We acknowledge that the UAV_RTK method was used only for research purposes and would not be used in practice, and therefore did not include this method in our cost analysis. In this exercise, we tracked the cost of surveying and estimating site-level vegetation height for 30 sites, each consisting of a 150-m-long plot on a seismic line. The estimated costs covered equipment, ancillary data purchase, data collection, and data processing. We assumed that a two-person field crew would be needed for data collection with the cost as follows (in Canadian dollars throughout): \$400/day per field technician; \$300/day per person for meals and accommodation during fieldwork; \$100/day for truck rental; and two extra days of salary, per diem, and truck rental for outbound and inbound travel from headquarters. We also assumed a maximum working day of 10 h, consisting of 1 h for travel from accommodation to the first plot of the day, 1 h for travel from the last plot of the day back to the accommodation site, and 1 h of travel among plots (which includes time for loading and unloading equipment). Given these assumptions, the cost of data collection in the field would be \$1500/day. We assumed the same salary cost for the technician processing data in the office (\$400/day).

Details of the three scenarios assessed for this cost analysis are summarized here:

(1) **Traditional vegetation surveys**. In this scenario, field crews perform traditional vegetation surveys in the field. Each plot takes 2 h for the survey plus 1 h between plots. Therefore, 30 plots take 90 h to complete, the equivalent of 9 days in the field. With the two additional travel days, the survey takes a total of 11 days.

(2) **UAV photogrammetry surveys with supplementary LiDAR**. The UAV_LiDAR method is equivalent to having a LiDAR-derived digital terrain model (DTM) with 1-m pixel size, which would be a cheaper source of terrain elevation than the LiDAR point cloud used in our study. If we assume that the 30 sites are all located within a single township within Alberta, the project could purchase a DTM derived from pre-existing LiDAR for this township for $100 [40], although the costs would be exponentially higher if no such high-quality data existed. The total equipment costs for this scenario are $1500 for the UAV, $9000 for the RTK GNSS, $500 for the camera, and $100 for accessories. However, this cost would be shared by other projects undertaken by the company. To estimate the equipment cost per day of fieldwork, we assume that the equipment becomes obsolete in 5 years and is used in 40 days of fieldwork per year, which yields a cost per field-day of $55.50. Each plot takes 1 h for UAV flight and GCP measurement, plus 1 h between plots. Therefore, 30 sites take a total of 60 h, equivalent to 6 days for the fieldwork, plus 2 days for outbound and inbound travel. This scenario also involves post-processing through Agisoft PhotoScan Professional Edition software, with a license cost of $5000/year. If we assume that this software will be used for five projects per year, then the software cost is $1000 per project. The data processing procedure includes aligning photos, generating point clouds, refining GCP locations, re-generating point clouds, and estimating vegetation parameters, all of which (except for refining GCP locations) are automatic and do not produce labor costs. Manually refining GCP locations, loading the data, and organizing outputs would take about 2 days of office work, at a total cost of $800.

(3) **Stand-alone UAV photogrammetry surveys**. In practice, detailed geo-referencing of point clouds can be skipped with the UAV_UAV method, because vegetation parameters can be computed in a relative space. That is, we can first generate a point cloud for a seismic line segment from the UAV photos corresponding to the segment, then clip the point cloud by a polygon representing the line segment using the orthophoto generated by the SfM software, and then apply the UAV_UAV method to each point of say a 1-m grid overlapping the polygon, and average the vegetation height of those points. Hence, in a scenario where repeated measurements are not sought after, geo-referencing is not necessary. Therefore, we assume that no GCPs are required in this scenario, and RTK GNSS equipment is therefore not needed. The total equipment costs are therefore $1500 for the UAV, $500 for the camera, and $100 for accessories. Assuming that the equipment is used for a minimum of 40 days of fieldwork per year for 5 years, the equipment cost per field-day is $10.50. Each plot takes 0.3 h for the UAV flight, plus 1 h between plots. Therefore, 30 sites take 39 h, equivalent to 4 field days, plus 2 days for travel. The survey takes a total of 6 days, with costs of $9000 for data collection and $63 for equipment. The cost of software is $1000. Regarding data processing, the difference between the UAV_UAV and UAV_LiDAR methods is that the process of refining GCP locations and re-generating point clouds is unnecessary for UAV_UAV. Therefore, loading the data and organizing outputs would take about 1 day of office work, at a cost of $400.

3. Results

3.1. Estimated Vegetation Height at the Point Level

Figure 9 shows histograms of estimated vegetation height errors at point level. Table 1 in supplement material summarizes the statistics comparing each of the three UAV-derived estimates of vegetation height to field measurements at the point level (n = 1743). The RMSEs for the UAV_RTK, UAV_LiDAR, and UAV_UAV methods were 28 cm, 31 cm, and 30 cm, respectively;

the normalized RMSE was 5% for all three methods; and the bias was 2 cm, –2 cm, and –4 cm, respectively. The correlation coefficients (Pearson's r, n = 1743) between field measurements and estimated vegetation heights were 0.76 for UAV_RTK, 0.72 for UAV_LiDAR, and 0.70 for UAV_UAV. Despite these strong results, significant differences remained between field measurements and remote-sensing estimates at the point level, as determined with paired-sample two-tailed z tests (p = 0.001 for UAV_RTK, p = 0.020 for UAV_LiDAR, and $p < 0.001$ for UAV_UAV).

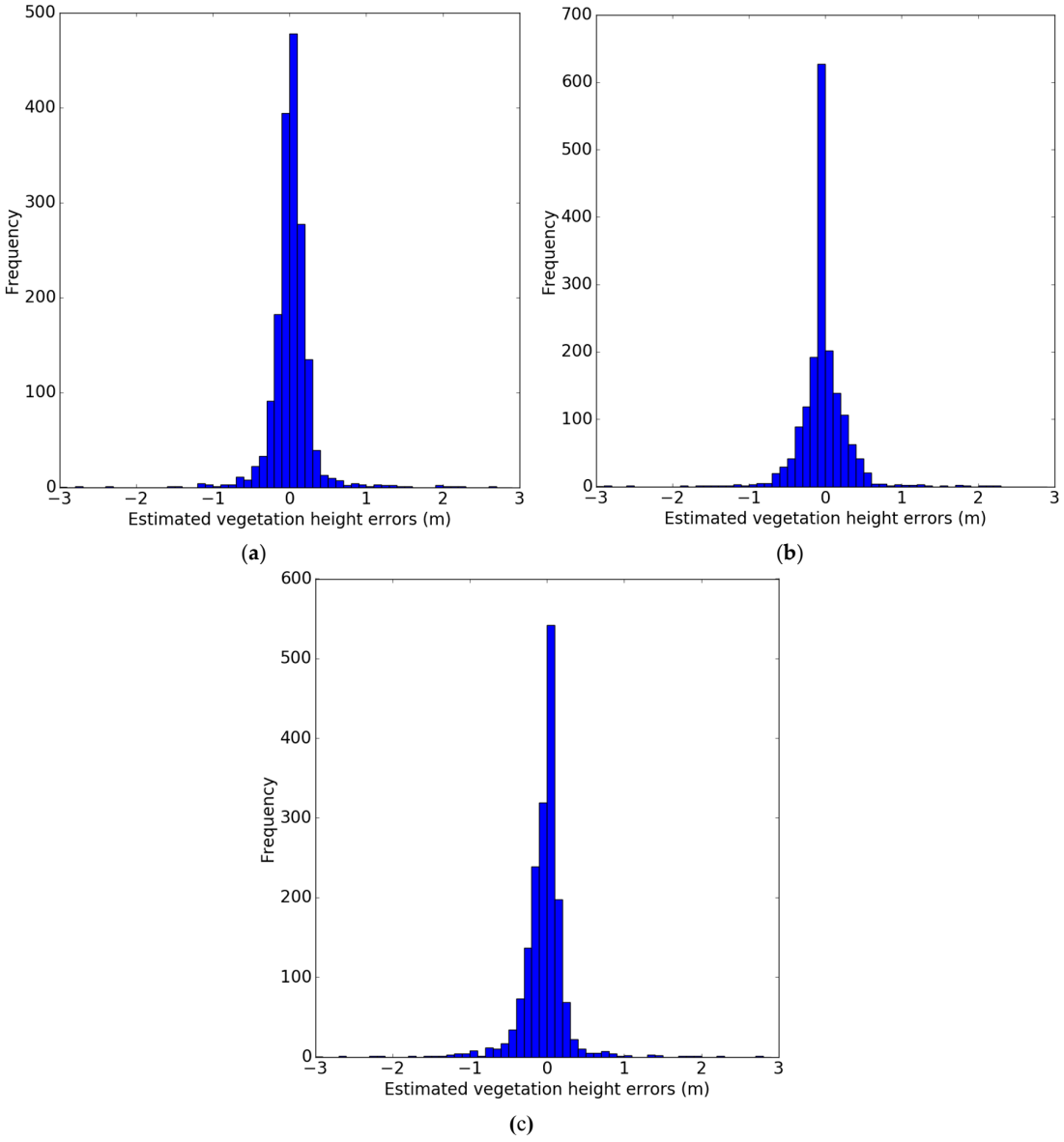

Figure 9. Histograms of estimated vegetation height errors at point level: (**a**) UAV_RTK; (**b**) UAV_LiDAR; (**c**) UAV_UAV.

Table 2 summarizes the RMSE, normalized RMSE, bias, Pearson's r, and p values of estimated vegetation heights by height strata: stratum I (low), 0–0.5 m; stratum II (medium), 0.51–2.0 m; and stratum III (high), >2.0 m. For all three remote-sensing techniques, the RMSE values were in the range of 0.2–0.46 m for strata I and II but rose above 0.8 m for stratum III, which suggests that our methods worked better in low to medium vegetation height strata. The three methods did not show large differences for the low and medium strata, whereas the RMSE and bias for the high stratum were significantly larger with UAV_UAV than with the other two methods. This indicates that the UAV_UAV

method would tend to underestimate vegetation height at the point level when the vegetation is high. The correlation coefficients of all sample points were higher than those of each stratum. Most of the *p* values were below 0.05, which suggests that the differences between field measurements and estimated vegetation heights were significant at the point level. Although two of the *p* values were greater than 0.05 for stratum III, we judge the estimated vegetation heights of stratum III at the point level to be unreliable, considering the small sample size, large RMSE, and low correlations observed.

Table 2. Root mean square error (RMSE), normalized RMSE (nRMSE), bias, Pearson's *r*, and *p* values of estimated vegetation heights at the point level, by stratum

Variable [1]	Method	RMSE (m)	nRMSE (%)	Bias	Pearson's *r*	*p* Value [2]
vh	UAV_RTK	0.28	5	0.02	0.76	0.001
	UAV_LiDAR	0.31	5	−0.02	0.72	0.02
	UAV_UAV	0.30	5	−0.04	0.70	<0.001
vh_I	UAV_RTK	0.22	7	0.07	0.39	<0.001
	UAV_LiDAR	0.24	8	0.03	0.38	<0.001
	UAV_UAV	0.20	6	0.03	0.33	<0.001
vh_{II}	UAV_RTK	0.40	11	−0.14	0.55	<0.001
	UAV_LiDAR	0.45	12	−0.20	0.54	<0.001
	UAV_UAV	0.46	12	−0.26	0.50	<0.001
vh_{III}	UAV_RTK	0.81	24	−0.30	0.09	0.062
	UAV_LiDAR	0.87	25	−0.33	0.11	0.053
	UAV_UAV	1.15	33	−0.66	−0.15	0.002

[1] vh: Overall vegetation height; vh_I: Vegetation height below 0.5 m; vh_{II}: Vegetation height between 0.51 m and 2 m; vh_{III}: Vegetation height above 2.0 m. RMSE: root-mean-square error. The sample sizes for vh, vh_I, vh_{II}, and vh_{III} were 1743, 1402, 315, and 26, respectively. [2] Two-tailed paired-sample *z* test between estimated vegetation height and field measurement. If $p < 0.05$, there was a significant difference between the means.

Our results suggest that the estimated vegetation height at the point level can achieve an RMSE of about 30 cm with or without supplemental terrain estimates. The performance of the three methods was very similar, which suggests that adding terrain data from field measurements or LiDAR did not significantly improve accuracy under the conditions of our study.

3.2. Estimated Mean Vegetation Height at the Site Level

Table 3 summarizes the statistics comparing the mean vegetation-height estimates for the three remote-sensing methods to field measurements aggregated to the site level ($n = 30$). The RMSEs for the UAV_RTK, UAV_LiDAR, and UAV_UAV methods were 11 cm, 15 cm, and 8 cm, respectively; the normalized RMSEs were 20%, 25%, and 26%, respectively; and the bias was 3 cm, –3 cm, and –2 cm, respectively. Paired-sample *z* tests (two-tailed) suggested that there were no significant differences between field-measured and remote-sensing estimates of mean vegetation height at the plot level ($p = 0.09$, 0.30, and 0.20 for UAV_RTK, UAV_LiDAR, and UAV_UAV, respectively). In addition, the correlation coefficients (Pearson's *r*) showed that all three methods strongly agreed with field measurements ($r = 0.96$, 0.91, and 0.95 for UAV_RTK, UAV_LiDAR, and UAV_UAV, respectively), as shown in the scatterplots (Figure 10).

Table 3. Root mean square error (RMSE), normalized RMSE (nRMSE), bias, Pearson's *r*, and *p* value for estimated mean vegetation heights at the site level (n = 30).

Statistics	UAV_RTK	UAV_LiDAR	UAV_UAV
RMSE (m)	0.11	0.15	0.08
nRMSE (%)	20	25	26
Bias (m)	0.03	−0.03	−0.02
Pearson's *r*	0.96	0.91	0.95
p value [1]	0.09	0.30	0.20

[1] For two-tailed paired-sample *z* test between estimated mean vegetation height and field measurement. If $p < 0.05$, there was a significant difference between the means.

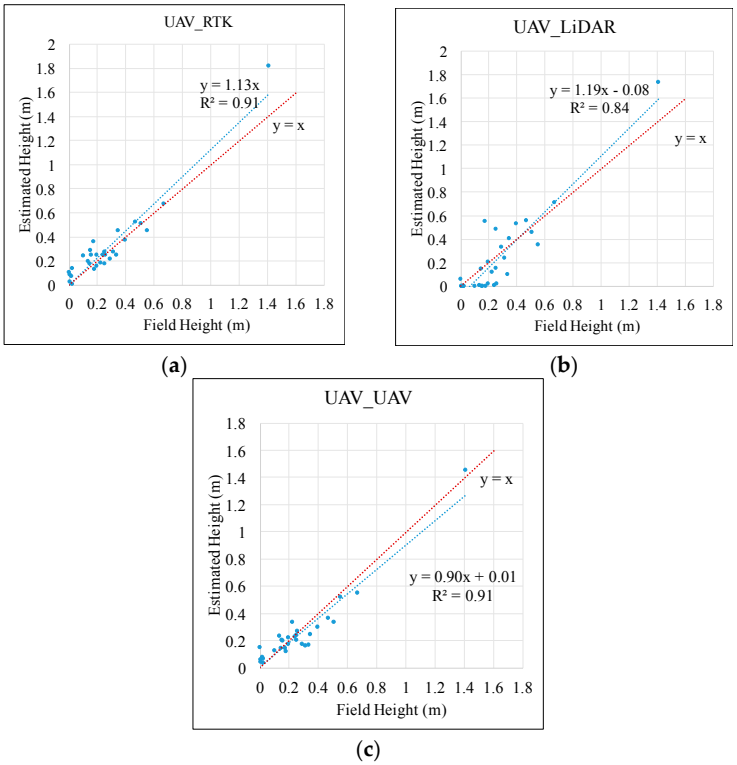

Figure 10. Estimated mean vegetation heights versus field measurements at the site level: (**a**) UAV_RTK; (**b**) UAV_LiDAR; (**c**) UAV_UAV.

Our results suggest that at the aggregated site level, UAV photogrammetry alone could achieve an RMSE of 8 cm. In addition, UAV photogrammetry data alone (UAV_UAV) achieved the same level of accuracy as methods supplemented with field-derived (UAV_RTK) or LiDAR-derived (UAV_LiDAR) estimates of terrain, which suggests that no such supplementation is needed.

3.3. Profile Comparisons

Comparisons for long-transect and cross-line transect profiles are shown in Figures 11 and 12, respectively. These visualizations corroborate the generally strong agreement between field measurements and remote sensing estimates of height reported in the quantitative assessments, with only a few instances of mismatch. In areas of relatively tall vegetation—for example the 80–90 m portion of the long transect in Figure 11 and the top-most cross-line transect in Figure 12a—we did observe some underestimation of vegetation height with the UAV_UAV method.

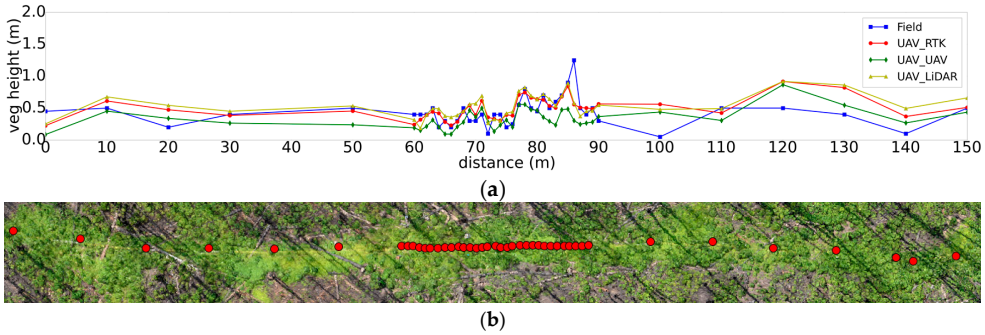

Figure 11. Example of long-transect profile comparison: (**a**) long-transect profile; and (**b**) locations of long-transect measurement stations (red dots).

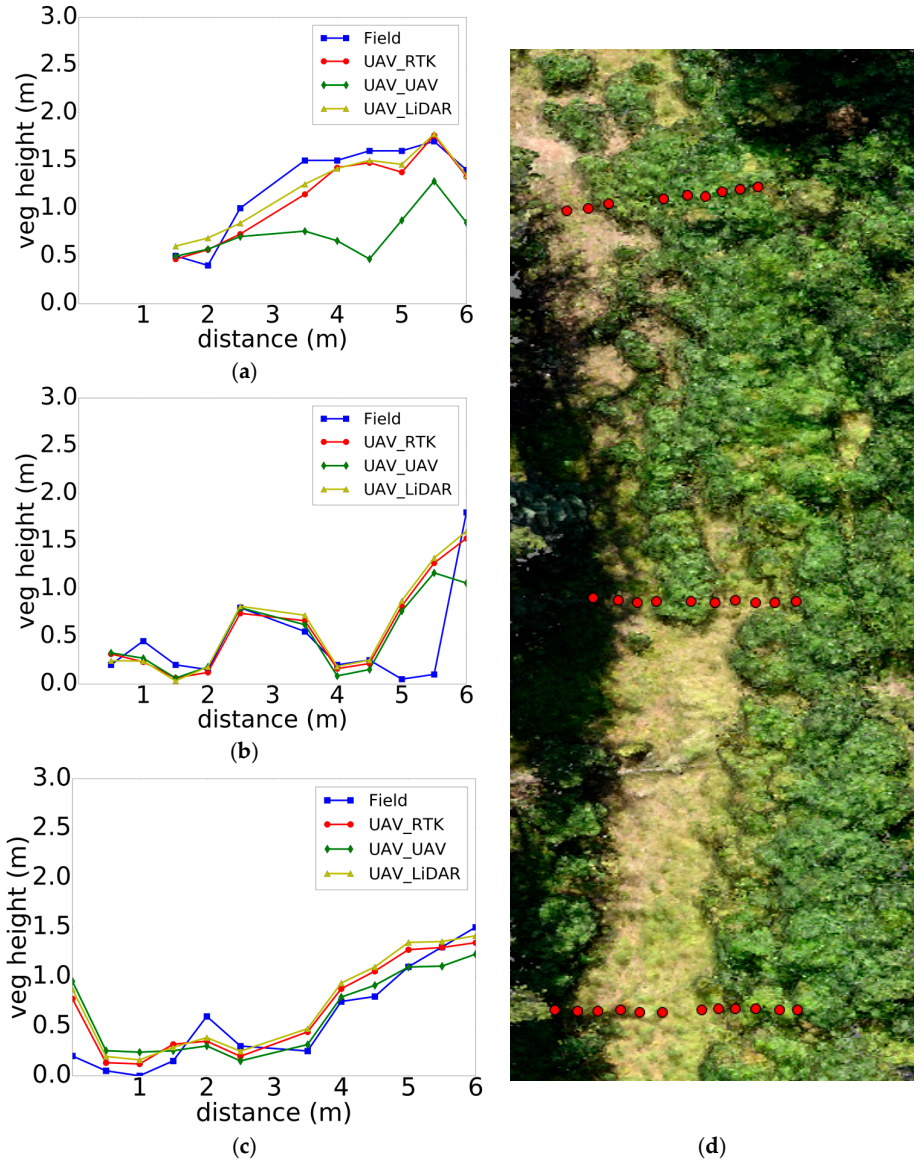

Figure 12. Example of cross-line transect profile comparison: (**a**) 60-m cross-line transect; (**b**) 75-m cross-line transect; (**c**) 90-m cross-line transect; (**d**) locations of cross-line transect measurement stations (red dots).

3.4. Optimal Search Radius for Lowest and Highest UAV Height Values around Sample Points

The relationship between the BSR and the RMSE of vegetation heights estimated with the UAV_UAV method is shown in Figure 13. At the site level, the best results (RMSE of 0.08 m) were obtained with a 1.0 m BSR. This same radius also performed very well at the point level, although the RMSE was slightly higher (1 cm) than that produced with a radius of 1.25 m. We decided to keep the smaller 1.0 m BSR, because it makes more plausible our assumption that terrain elevation does not change significantly within the search radius. For the sake of consistency, we used the same radius for heights estimated with UAV_LiDAR.

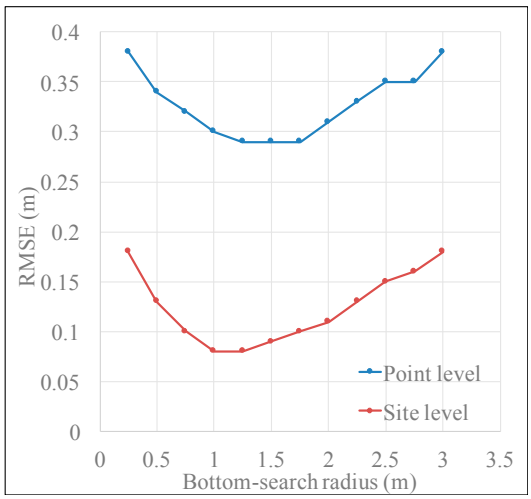

Figure 13. Bottom-search radius versus RMSE of vegetation-height estimates using the UAV_UAV method.

The relation between TSR and the RMSE of height estimates at the site level for all three methods is shown in Figure 14. The best results for UAV_UAV (RMSE of 0.08 m) were obtained with 0.2 m as the TSR. For UAV_LiDAR the best results (RMSE of 0.15 m) were obtained with a search radius of 0.2 m or smaller. Therefore, having in mind an operational scenario with no ancillary data (LiDAR or RTK), we ascertained that the choice of 0.2 m for the TSR was indeed optimal.

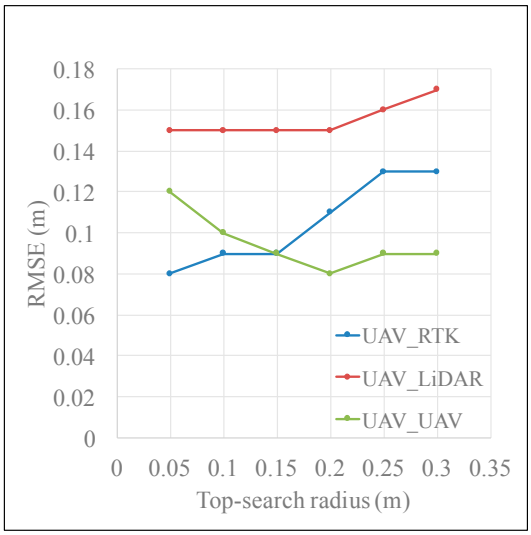

Figure 14. Top-search radius versus RMSE of height estimates (site level).

3.5. Cost Analysis

The costs of the three scenarios are summarized in Table 4. According to this analysis, using UAV photogrammetry alone to produce site-level vegetation parameters (total cost $10,463) would be substantially less expensive than traditional field surveys (total cost $16,900), even with added equipment and processing costs. Supplementing photogrammetry data with a high-quality DTM would increase total cost to $14,344, largely because of the increased data-collection costs associated with ground control and RTK GNSS surveys required to finely co-register the point cloud to the LiDAR digital elevation model (DEM). As previously noted, however, this additional step was not necessary for the low-vegetation sites that we assessed.

Table 4. Cost analysis for traditional, UAV_LiDAR, and UAV_UAV methods (data are in Canadian dollars).

Method	Data Purchase	Equipment	Data Collection	Software	Data Processing	Total Cost
Traditional	0	0	$16,500	0	$400	$16,900
UAV_LiDAR	$100	$444	$12,000	$1000	$800	$14,344
UAV_UAV	0	63	$9,000	$1000	$400	$10,463

4. Discussion

Our results (paired-sample two-tailed z tests, $p = 0.20$) show that at the aggregated site level, point clouds derived from UAV photogrammetry alone (the UAV_UAV method) could replace traditional field-based vegetation surveys of mean vegetation height across the range of conditions assessed in this study, with an RMSE less than 10 cm. At the point level, however, significant differences remain between field surveys and point clouds derived from UAV photogrammetry. Regardless of point-level or site-level estimates, point clouds derived from UAV photogrammetry alone (UAV_UAV) achieved the same level of accuracy as methods supplemented with field-derived (UAV_RTK) or LiDAR-derived (UAV_LiDAR) estimates of terrain elevation, indicating that an ancillary data set may not be necessary for estimating the height of low vegetation that does not completely cover the ground. Our cost analysis indicated that using UAV point clouds alone offers substantial cost savings over traditional field vegetation surveys.

Our study is novel in a number of respects. First, earlier studies characterizing vegetation with UAVs often used LiDAR data to estimate terrain elevation and normalize UAV-based point clouds [27,41,42]. In this study, in addition to the LiDAR-based method, we assessed two alternative methods of estimating terrain elevation for normalization: field-measured RTK GNSS surveys (UAV_RTK) and UAV photogrammetry alone (UAV_UAV). Second, previous studies have tended to estimate vegetation parameters at the plot or stand level [27,43]. In this study, we used a point-intercept strategy and compared UAV-based estimates and field measurements at both the point level and the plot level. Finally, many earlier studies have used LiDAR data to characterize vegetation in forests [15,20]; although other researchers have started to explore the use of UAVs in mature forests [44,45], very few studies have characterized vegetation in areas of forest disturbance [41,46]. To the best of our knowledge, ours is the first dealing with linear disturbances.

Although the UAV_UAV method produced good estimates of vegetation parameters in places when the vegetation was not too dense, it is likely that UAV photogrammetry alone would tend to underestimate vegetation height in areas of dense vegetation, which would in turn tend to occlude the ground from this passive remote-sensing technique [42]. Under these conditions, and considering accuracy and cost, UAV photogrammetry supplemented with existing LiDAR (UAV_LiDAR) may be a better choice. Once again, though, this problem was not observed regularly across the range of conditions that we assessed.

There were several sources of error in this study. First, RTK measurements, though accurate in most cases, may have relatively large errors when vegetation is high and dense. The RTK GNSS

survey technique relies on good communication between the base station and the rover, as well as good reception of satellite signals. When the receiver is occluded by dense vegetation, RTK cannot provide a fixed position due to insufficient number of satellites that are visible, and low accuracy may result. This problem exists in measuring both the coordinates of GCPs and the sample points on the transects. To reduce this error, we recorded measurements only under conditions where the solution of RTK GNSS could be fixed. Vertical errors caused by RTK GNSS would only affect the UAV_RTK method. However, horizontal errors of RTK GNSS would affect all three of the methods that we explored, particularly at the point level. This may have contributed to some outliers between the field- and remote sensing-derived estimates of height at the point level. Second, UAV photogrammetry supplemented with LiDAR (UAV_LiDAR) requires accurate co-registration between the two data sets. Here, the absolute accuracy of the LiDAR data set was reported at 30 cm, which may have contributed some error.

In the future, our workflows should be tested for more sites and under other different environments and vegetation recovery status. In addition, further research should explore the factors affecting the accuracy of vegetation-parameter estimates and develop methods to improve accuracy. Among the possible factors at play are image quality (e.g., resolution, contrast, sharpness), flight and lighting conditions, vegetation density, the presence of shadows on the lines, and phenological conditions. Also, further research should investigate strategies for reducing the processing time required to generate point clouds. In our study, producing high-density point clouds from images required substantial amounts of computational time for each site. Finally, future research should also explore methods of estimation of a wider set of vegetation characteristics, such as species composition, using UAV technology.

5. Conclusions

In this study, we used a point-intercept sampling strategy to evaluate the accuracy of estimated vegetation heights using photogrammetric point clouds derived from UAV imagery. Three normalization methods were used to estimate UAV-based vegetation height: (1) UAV_RTK, where RTK GNSS equipment was used to measure terrain elevation; (2) UAV_LiDAR, where the lowest pre-existing LiDAR point within a search radius from the sample point was used to estimate terrain elevation; and (3) UAV_UAV, where the lowest UAV point within a search radius from the sample point was used to estimate terrain elevation. Our results (paired-sample two-tailed z tests, $p = 0.20$) show that at the aggregated site or plot level, there was no significant difference between UAV- and field-surveyed height estimates, suggesting that UAV photogrammetry alone (the UAV_UAV method) could replace traditional field-based vegetation surveys of mean vegetation height across the range of conditions assessed in this study, with an RMSE less than 10 cm. Significant differences between UAV-based and field-surveyed vegetation heights were observed at the point level. At both scales (point level and site level), UAV photogrammetry alone achieved the same level of accuracy as the methods supplemented with field-derived (UAV_RTK) or LiDAR-derived (UAV_LiDAR) estimates of terrain elevation. Cost analysis indicates that using UAV-based point clouds is more cost-effective than traditional field vegetation surveys.

These results contribute to the development of repeatable, cost-effective, and fine-scale vegetation-recovery monitoring strategies for areas of forest disturbance based on UAV photogrammetry.

Supplementary Materials: The following are available online at www.mdpi.com/2072-4292/9/12/1257/s1.

Acknowledgments: This research was supported by a Natural Sciences and Engineering Research Council of Canada Collaborative Research and Development Grant (CRDPJ 469943-14) in conjunction with Alberta-Pacific Forest Industries, Cenovus Energy, and ConocoPhillips Canada. Additional support was received from Natural Resources Canada (project PERD 1C03.015). Thank you to Jennifer Hird for her contributions to the field protocol, Corey Feduck for piloting of the UAV, and other BERA team members for assisting with various aspects of data collection: Man Fai Wu, Jaren Koning, Vince Zafra, Natalie Sanchez, Michael Bodnar, Erica Graham, Tobias Tan, and Angelo Filicetti. We also acknowledge three anonymous reviewers for their constructive suggestions, which helped to improve the manuscript.

Author Contributions: Gregory J. McDermid, Guillermo Castilla, and Julia Linke conceived the experiments and revised the paper substantially; Shijuan Chen performed the experiments, collected and analyzed the data, and wrote the first draft of the paper.

Conflicts of Interest: The authors declare no conflict of interest. The funding sponsors had no role in the design of the study; in the collection, analysis, or interpretation of data; in the writing of the manuscript; or in the decision to publish the results.

References

1. Festa-Bianchet, M.; Ray, J.C.; Boutin, S.; Côté, S.D.; Gunn, A. Conservation of caribou (*Rangifer tarandus*) in Canada: An uncertain future. *Can. J. Zool.* **2011**, *89*, 419–434. [CrossRef]
2. Environment and Climate Change Canada. *Report on the Progress of Recovery Strategy Implementation for the Woodland Caribou (Rangifer tarandus caribou), Boreal population in Canada for the Period 2012–2017. Species at Risk Act Recovery Strategy Series*; Environment and Climate Change Canada: Ottawa, ON, Canada, 2017.
3. Salmo Consulting Inc.; Athabasca Landscape Team. *Athabasca Caribou Landscape Management Options Report*; Alberta Caribou Committee Governance Board: Edmonton, AB, Canada, 2009.
4. Ritchie, C.; George, P. *Boreal Caribou Habitat Restoration*; Government of British Columbia: Victoria, BC, Canada, 2012.
5. Pyper, M.; Nishi, J.; McNeil, L. *Linear Feature Restoration in Caribou Habitat: A Summary of Current Practices and a Roadmap for Future Programs*; Fuse Consulting: Calgary, AB, Canada, 2014.
6. Latham, A.D.M.; Latham, M.C.; Knopff, K.H.; Hebblewhite, M.; Boutin, S. Wolves, white-tailed deer, and beaver: Implications of seasonal prey switching for woodland caribou declines. *Ecography* **2013**, *36*, 1276–1290. [CrossRef]
7. Latham, A.D.M.; Latham, M.C.; Boyce, M.S.; Boutin, S. Movement responses by wolves to industrial linear features and their effect on woodland caribou in northeastern Alberta. *Ecol. Appl.* **2011**, *21*, 2854–2865. [CrossRef]
8. Van Rensen, C.K.; Nielsen, S.E.; White, B.; Vinge, T.; Lieffers, V.J. Natural regeneration of forest vegetation on legacy seismic lines in boreal habitats in Alberta's oil sands region. *Biol. Conserv.* **2015**, *184*, 127–135. [CrossRef]
9. Dickie, M.; Serrouya, R.; Demars, C.; Cranston, J.; Boutin, S. Evaluating functional recovery of habitat for threatened woodland caribou. *Ecosphere* **2017**, *9*. [CrossRef]
10. Golder Associates Ltd. *Caribou Habitat Restoration Pilot Study. Submitted to: ConocoPhillips Canada, Suncor Energy, and the Canadian Association of Petroleum Producers*; Golder Associates Ltd.: Hong Kong, China, 2009.
11. Alberta Government. *Alberta Timber Harvest Planning and Operating Ground Rules Framework for Renewal*; Government of Alberta: Edmonton, AB, Canada, 2016.
12. Magnussen, S.; Russo, G. Uncertainty in photo-interpreted forest inventory variables and effects on estimates of error in Canada's National Forest Inventory. *For. Chron.* **2012**, *88*, 439–447. [CrossRef]
13. Lefsky, M.A. A global forest canopy height map from the Moderate Resolution Imaging Spectroradiometer and the Geoscience Laser Altimeter System. *Geophys. Res. Lett.* **2010**, *37*. [CrossRef]
14. McRoberts, R.E.; Cohen, W.B.; Næsset, E.; Stehman, S.V.; Tomppo, E.O. Using remotely sensed data to construct and assess forest attribute maps and related spatial products. *Scand. J. For. Res.* **2010**, *25*, 340–367. [CrossRef]
15. Weber, T.C.; Boss, D.E. Use of LiDAR and supplemental data to estimate forest maturity in Charles County, MD, USA. *For. Ecol. Manag.* **2009**, *258*, 2068–2075. [CrossRef]
16. Persson, H.J.; Perko, R. Assessment of boreal forest height from WorldView-2 satellite stereo images. *Remote Sens. Lett.* **2016**, *7*, 1150–1159. [CrossRef]
17. Pan, Y.; Birdsey, R.A.; Phillips, O.L.; Jackson, R.B. The structure, distribution, and biomass of the world's forests. *Annu. Rev. Ecol. Evol. Syst.* **2013**, *44*, 593–622. [CrossRef]
18. Bouvier, M.; Durrieu, S.; Fournier, R.A.; Renaud, J.-P. Generalizing predictive models of forest inventory attributes using an area-based approach with airborne LiDAR data. *Remote Sens. Environ.* **2015**, *156*, 322–334. [CrossRef]
19. Breidenbach, J.; Nothdurft, A.; Kändler, G. Comparison of nearest neighbour approaches for small area estimation of tree species-specific forest inventory attributes in central Europe using airborne laser scanner data. *Eur. J. For. Res.* **2010**, *129*, 833–846. [CrossRef]

20. Estornell, J.; Ruiz, L.A.; Velázquez-Martí, B.; Fernández-Sarría, A. Estimation of shrub biomass by airborne LiDAR data in small forest stands. *For. Ecol. Manag.* **2011**, *262*, 1697–1703. [CrossRef]
21. Vastaranta, M.; Holopainen, M.; Yu, X.; Hyyppä, J.; Hyyppä, H.; Viitala, R. Predicting stand-thinning maturity from airborne laser scanning data. *Scand. J. For. Res.* **2011**, *26*, 187–196. [CrossRef]
22. Whitehead, K.; Hugenholtz, C.H.; Myshak, S.; Brown, O.; LeClair, A.; Tamminga, A.; Barchyn, T.E.; Moorman, B.; Eaton, B. Remote sensing of the environment with small unmanned aircraft systems (UASs), part 2: Scientific and commercial applications 1. *J. Unmanned Veh. Syst.* **2014**, *2*, 86–102. [CrossRef]
23. Lisein, J.; Pierrot-Deseilligny, M.; Bonnet, S.; Lejeune, P. A photogrammetric workflow for the creation of a forest canopy height model from small unmanned aerial system imagery. *Forests* **2013**, *4*, 922–944. [CrossRef]
24. Hardin, P.J.; Jensen, R.R. Small-scale unmanned aerial vehicles in environmental remote sensing: Challenges and opportunities. *GISci. Remote Sens.* **2011**, *48*, 99–111. [CrossRef]
25. Dandois, J.P.; Ellis, E.C. Remote sensing of vegetation structure using computer vision. *Remote Sens.* **2010**, *2*, 1157–1176. [CrossRef]
26. Järnstedt, J.; Pekkarinen, A.; Tuominen, S.; Ginzler, C.; Holopainen, M.; Viitala, R. Forest variable estimation using a high-resolution digital surface model. *ISPRS J. Photogramm. Remote Sens.* **2012**, *74*, 78–84. [CrossRef]
27. Puliti, S.; Ørka, H.O.; Gobakken, T.; Næsset, E. Inventory of small forest areas using an unmanned aerial system. *Remote Sens.* **2015**, *7*, 9632–9654. [CrossRef]
28. White, J.C.; Wulder, M.A.; Vastaranta, M.; Coops, N.C.; Pitt, D.; Woods, M. The utility of image-based point clouds for forest inventory: A comparison with airborne laser scanning. *Forests* **2013**, *4*, 518–536. [CrossRef]
29. Dandois, J.P.; Ellis, E.C. High spatial resolution three-dimensional mapping of vegetation spectral dynamics using computer vision. *Remote Sens. Environ.* **2013**, *136*, 259–276. [CrossRef]
30. Whitehead, K.; Hugenholtz, C.H.; Myshak, S.; Brown, O.; LeClair, A.; Tamminga, A.; Barchyn, T.E.; Moorman, B.; Eaton, B. Remote sensing of the environment with small unmanned aircraft systems (UASs), part 1: A review of progress and challenges. *J. Unmanned Veh. Syst.* **2014**, *2*, 86–102. [CrossRef]
31. Vastaranta, M.; Wulder, M.A.; White, J.C.; Pekkarinen, A.; Tuominen, S.; Ginzler, C.; Kankare, V.; Holopainen, M.; Hyyppä, J.; Hyyppä, H. Airborne laser scanning and digital stereo imagery measures of forest structure: Comparative results and implications to forest mapping and inventory update. *Can. J. Remote Sens.* **2013**, *39*, 382–395. [CrossRef]
32. Natural Regions Committee. *Natural Regions and Subregions of Alberta*; Downing, D.J.; Pettapiece, W.W. (Compiler) Publ. No. T/852; Government of Alberta: Edmonton, AB, Canada, 2006.
33. Donahue, B.; Wentzel, J.; Berg, R. *Guidelines for RTK/RTN GNSS Surveying in Canada*; Version 1.1; Natural Resources Canada: Ottawa, ON, Canada, 2013.
34. Hird, J.N.; Nielsen, S.; McDermid, G.; Tan, T. *BERA Project: Baseline Field Data Collection Protocols, Version 2016-07-15*; Boreal Ecosystem Recovery and Assessment (BERA): Calgary, AB, Canada, 2016.
35. Agisoft. Agisoft Photoscan User Manual. Available online: http://www.agisoft.com/pdf/photoscan-pro_1_2_en.pdf (accessed on 2 December 2017).
36. Schenk, T. Section 6.2: Digital phogrammetric workstations. In *Introduction to Photogrammetry*; Ohio State University, Department of Civil and Environmental Enginering and Geodetic Science: Columbus, OH, USA, 2005; pp. 79–95.
37. Westoby, M.J.; Brasington, J.; Glasser, N.F.; Hambrey, M.J.; Reynolds, J.M. "Structure-from-Motion" photogrammetry: A low-cost, effective tool for geoscience applications. *Geomorphology* **2012**, *179*, 300–314. [CrossRef]
38. Triggs, B.; McLauchlan, P.F.; Hartley, R.I.; Fitzgibbon, A.W. Bundle Adjustment—A Modern Synthesis. In *Vision Algorithms: Theory and Practice, Proceedings of the International Workshop on Vision Algorithms, Corfu, Greece, 21–22 Septem 2000*; Lecture Notes in Computer Science; Triggs, B., Zisserman, A., Szeliski, R., Eds.; Springer: Berlin/Heidelberg, Germany, 2000; Volume 1883.
39. Isenburg, M. LAStools—Efficient Tools for LiDAR Processing. 2013. Available online: http://lastools.org (accessed on 2 December 2017).
40. AltaLIS. LiDAR15 DEM. Available online: http://www.altalis.com/products/terrain/lidar15_dem.html (accessed on 2 December 2017).

41. Hird, J.N.; Montaghi, A.; McDermid, G.J.; Kariyeva, J.; Moorman, B.J.; Nielsen, S.E.; McIntosh, A.C.S. Use of unmanned aerial vehicles for monitoring recovery of forest vegetation on petroleum well sites. *Remote Sens.* **2017**, *9*. [CrossRef]
42. White, J.C.; Stepper, C.; Tompalski, P.; Coops, N.C.; Wulder, M.A. Comparing ALS and image-based point cloud metrics and modelled forest inventory attributes in a complex coastal forest environment. *Forests* **2015**, *6*, 3704–3732. [CrossRef]
43. Maltamo, M.; Bollandsås, O.; Næsset, E.; Gobakken, T.; Packalén, P.; Bollandsås, O.M.; Næsset, E.; Gobakken, T.; Packalén, P. Different plot selection strategies for field training data in ALS-assisted forest inventory. *Forestry* **2011**, *84*, 23–31. [CrossRef]
44. Jensen, J.L.R.; Mathews, A.J. Assessment of image-based point cloud products to generate a bare earth surface and estimate canopy heights in a woodland ecosystem. *Remote Sens.* **2016**, *8*. [CrossRef]
45. Goodbody, T.R.H.; Coops, N.C.; Marshall, P.L.; Tompalski, P.; Crawford, P. Unmanned aerial systems for precision forest inventory purposes: A review and case study. *For. Chron.* **2017**, *93*, 71–81. [CrossRef]
46. Zahawi, R.A.; Dandois, J.P.; Holl, K.D.; Nadwodny, D.; Reid, J.L.; Ellis, E.C. Using lightweight unmanned aerial vehicles to monitor tropical forest recovery. *Biol. Conserv.* **2015**, *186*, 287–295. [CrossRef]